Hyper-Raman and Raman studies on the phase transition of ferroelectric $LiTaO_3$

Y. Tezuka and S. Shin
Synchrotron Radiation Laboratory, Institute for Solid State Physics, University of Tokyo, 3-2-1 Midori-cho, Tanashi, Tokyo 188, Japan

M. Ishigame
Research Institute for Scientific Measurement, Tohoku University, 2-1-1 Katahira, Aoba-ku, Sendai 980, Japan
(Received 24 August 1993; revised manuscript received 8 November 1993)

Hyper-Raman and Raman spectra of ferroelectric $LiTaO_3$ are observed in the temperature range from 14 to 1200 K, which includes the phase-transition temperature at about 890 K. In the ferroelectric phase, no evidence of the softening of the A_1 phonon is found in the spectra. However, the hyper-Raman spectra show a strong Debye-type relaxational mode in both phases. The hyper-Raman spectra clearly show that the phase transition of $LiTaO_3$ is of the order-disorder type. The anomalous line shape of an A_1 phonon band at 203 cm^{-1} is interpreted in terms of the coupling between this phonon and the relaxational modes. The coupling model also explains the difference between the line shapes of the Raman and hyper-Raman spectra.

I. INTRODUCTION

It is well known that lithium tantalate ($LiTaO_3$) undergoes a phase transition from the high-temperature paraelectric (PE) to the low-temperature ferroelectric (FE) phase at about $T_C = 890$ K. The Curie temperature T_C of $LiTaO_3$, however, varies from 810 to 970 K with its growth conditions and stoichiometry.[1] The crystal structure of $LiTaO_3$ is uniaxial trigonal belonging to the C_{3v} point group in the FE phase and to the centrosymmetric D_{3d} point group in the PE phase. The optical properties as well as the detailed crystal structure of $LiTaO_3$ have been studied extensively in order to elucidate the mechanism of the phase transition.[2-11] However, there are some discrepancies among these results. Johnston and Kaminow measured the temperature dependence of the Raman spectra of $LiTaO_3$ and reported a soft phonon with the $A_1(Z)$ symmetry in the FE phase.[2] Sevoin and Gervais also reported the soft phonon in both phases by means of infrared reflectivity measurement.[3]

On the other hand, Raptis assigned the lattice modes of $LiTaO_3$ in both phases, by means of Raman scattering for several scattering configurations.[4] However, no evidence of the softening of the phonon was found. Further, Jayaraman and Ballman investigated the pressure dependence of the Raman spectra of $LiTaO_3$ in the FE phase. In the pressure range from 1 to 1×10^{10} Pa, they found that the frequencies of all modes increase with increasing pressure, but did not observe any phonon softening.[5] They concluded that the phase transition of $LiTaO_3$ is not of the displacive type but of the order-disorder type.

Penna, Porto, and Wiener-Avnear found a Debye-like central peak in the FE phase by means of Raman scattering.[6] Further, from the temperature dependence of Raman spectra, they found an anomalous polariton dispersion of $A_1(Z)$ phonon modes near T_C in the FE phase, and suggested that dynamical domain fluctuations occur in $LiTaO_3$.[7]

By neutron-scattering measurements, Samuelsen and Grande showed that the temperature dependence of the spontaneous polarization P_s, which is obtained from the scattering intensity, can be explained in terms of the gradual ordering of Li ions.[8] Abrahams *et al.* found that, above T_C, Li ions occupy two equivalent positions on either side of the oxygen plane with equal probability.[9] On the other hand, Chowdhury, Peckham, and Saunderson reported that they failed to observe any softening of the phonon mode.[10]

Recently, Tomeno and Matsumura measured the dielectric constants and reported that $LiTaO_3$ has a large Curie constant of 1.43×10^5 K, which supports the displacive phase transition.[11] However, they also reported a dispersion of the dielectric constants, which is caused by Li-ion motion. They though that there is a coupling between the soft phonon and the relaxational mode.

The aim of this paper is to study the origin of the phase transition of $LiTaO_3$ by means of hyper-Raman and Raman scattering. It is essential to find the "soft mode." If the phase transition of the displacive type, the "soft mode" is the "soft phonon." In this paper, the "soft phonon" is used as a phonon whose frequency decreases rapidly to zero with temperature as the phase transition is approached. On the other hand, if the phase transition is of the order-disorder type, it is the Debye-type relaxational "central mode." The "central mode" is distinguished from the overdamped phonon whose spectrum has a peak at zero frequency. It is important to observe the "soft mode" in the PE phase in order to study the mechanism of the phase transition, since there are serious inconsistencies among the studies in FE phase as described above. In the PE phase, however, the "soft mode" is not observed by Raman scattering because of the selection rules.

Hyper-Raman scattering (HRS) is well known as the nonlinear Raman scattering with two exciting photons and one scattered photon. One of the most important

features of hyper-Raman scattering is the selection rule that all infrared-active modes are also active in hyper-Raman scattering. That is, the ferroelectric A_1 mode is always active in hyper-Raman scattering. Then, the corresponding A_{2u} mode in the PE phase will be active in the hyper-Raman spectrum. Furthermore, the measurement of the hyper-Raman scattering is easier than the infrared (IR) measurement at high temperatures. Thus, the hyper-Raman scattering is very powerful for the study of the phase transition of $LiTaO_3$.

II. EXPERIMENT

The poled single crystal of $LiTaO_3$ was commercially obtained from Yamaju ceramics K.K. Optically polished samples were used with the dimensions of about $4\times5\times6$ mm^3.

Figure 1 shows the experimental system for Raman and hyper-Raman measurements. As the light source of the exciting radiation of the hyper-Raman scattering measurements, an acoustic Q-switched Nd-YAG laser was used at a wavelength of 1064 nm. Its peak power was about 6 kW with pulse width of about 100 nsec and a pulse repetition rate of 9 kHz. For the Raman scattering measurements, an Ar-ion laser was used at 488.0 nm with an average power of about 0.7 W.

A focusing lens with the rather long focal distance of $f=200$ mm was used to avoid dielectric break down of the crystals for the hyper-Raman scattering, while an $f=100$-mm lens was used for the Raman scattering measurements. In order to remove the elastic scattering from the sample surface, a 90° scattering geometry was mainly used. On the other hand, backscattering geometry was used in the high-temperature region over 1100 K. In this geometry, the slit of the monochromator can be reduced in height and intercept the thermal emission from the sample. A double-grating monochromator (JASCO, CT-1000D) was employed. The scattering light was collected by a condenser lens into the entrance slit of the monochromator.

The hyper-Raman scattering light was very weak so that a very sensitive multichannel detector PIAS (Ref. 12) (Photon-counting level Image Acquisition System, Hamamatsu Photonics, K.K.) was used. The PIAS has the two-dimensional position-sensitive detector (PSD). The dark count level due to the thermal noise of the detector and the thermal emission of the high-temperature sample is reduced down to about $\frac{3}{1000}$ by the gated-photon counting synchronized with the laser pulses. Then, it is possible to detect such weak signals as a few counts per one day for one channel. The spectral resolution of this hyper-Raman scattering system is about 1 cm^{-1}. The PIAS could not detect intensive signals because its detector is very sensitive for such signals.

A photomultiplier was used in the Raman scattering measurements, since the Rayleigh light is very strong. The spectral resolution is about 1 cm^{-1}.

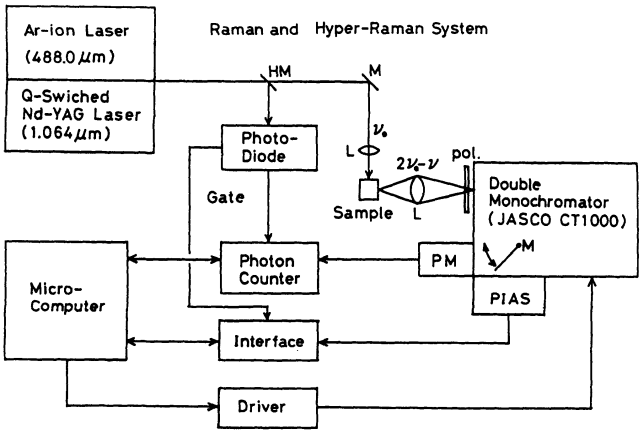

FIG. 1. Schematic diagrams of experimental arrangement.

III. GROUP-THEORETICAL ANALYSIS

A. Unit cell

The $LiTaO_3$ crystal has two molecules (10 ions) in a primitive unit cell. Figure 2(a) shows the unit-cell structure of $LiTaO_3$ crystal. Figure 2(b) shows the positions of Li and Ta ions in this crystal in the FE phase. Figures 2(c) and 2(d) show the two types of the models for the positions of Li and Ta ions in the PE phase.[9,10]

B. Paraelectric phase

In the PE phase, $LiTaO_3$ has a centrosymmetric point group symmetry D_{3d}. Then, the optical vibrational modes are distributed among irreducible representations as follows:

$$\Gamma_{\text{opt}}=A_{1g}+3A_{2g}+4E_g+2A_{1u}+3A_{2u}(Z)+5E_u(X,Y)\ ,$$

where the A_{1g} and E_g modes are only Raman active, the A_{2u} and E_u modes are infrared and hyper-Raman active, and the silent A_{1u} modes are only hyper-Raman active. The selection rules of the hyper-Raman scattering is described elsewhere.[13] The Ta ion is located at a site shown by a dashed line, but the position of the Li ion is not definite. In the case of the displacive-type phase-transition mechanism, the Li ion must be located at a site in an oxygen plane as shown in Fig. 2(c). In the case of

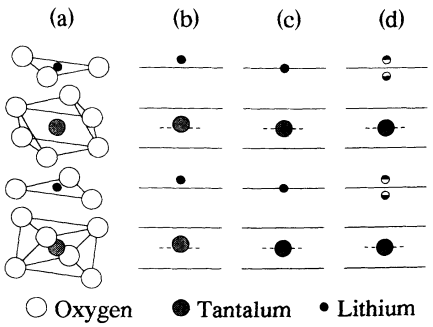

FIG. 2. (a) Structure of lithium tantalate. (b) Positions of Li and Ta ions in FE phase. (c) and (d) Positions of Li and Ta ions in the PE phase in the case of displacive-type phase transition (c) and order-disorder-type phase transition (d). Solid lines are the oxygen-ion plane. Dashed lines are the middle of the oxygen plane where the Ta ion is located.

the order-disorder-type phase-transition mechanism, however, it is considered to be at a site shifted to either side of the oxygen plane as shown in Fig. 2(d).[9]

Since the direction of the spontaneous polarization is along the Z axis, the soft mode should belong to $A_{2u}(Z)$ symmetry in the PE phase. Then, the soft mode is active for hyper-Raman scattering but not for Raman scattering in the PE phase. In the PE phase, the Raman tensors are

$$A_{1g}=\begin{bmatrix} a & \cdot & \cdot \\ \cdot & a & \cdot \\ \cdot & \cdot & b \end{bmatrix},$$

$$E_g(X)=\begin{bmatrix} c & \cdot & \cdot \\ \cdot & -c & d \\ \cdot & d & \cdot \end{bmatrix},$$

$$E_g(Y)=\begin{bmatrix} \cdot & c & d \\ c & \cdot & \cdot \\ d & \cdot & \cdot \end{bmatrix},$$

and the hyper-Raman tensors are

$$A_{1u}=\begin{bmatrix} a & -a/3 & \cdot & \cdot & \cdot & \cdot \\ \cdot & \cdot & \cdot & \cdot & \cdot & -a/3 \\ \cdot & \cdot & \cdot & \cdot & \cdot & \cdot \end{bmatrix},$$

$$A_{2u}=\begin{bmatrix} \cdot & \cdot & \cdot & \cdot & b & -d/3 \\ -d/3 & d & \cdot & b & \cdot & \cdot \\ b & b & c & \cdot & \cdot & \cdot \end{bmatrix},$$

$$E_u(X)=\begin{bmatrix} e & e & g & \cdot & -f & \cdot \\ \cdot & \cdot & \cdot & f & \cdot & e \\ -f & f & \cdot & \cdot & g & \cdot \end{bmatrix},$$

$$E_u(Y)=\begin{bmatrix} \cdot & \cdot & \cdot & f & \cdot & e \\ e & e & g & \cdot & f & \cdot \\ \cdot & \cdot & \cdot & g & \cdot & f \end{bmatrix}.$$

Since the crystal has the centrosymmetry in the PE phase, second harmonic generation (SHG) is forbidden at any configuration. Thus, the strong elastic scattering at $2\omega_0$ by the SHG, which is often called "hyper-Rayleigh scattering," will not be observed. So, the hyper-Raman scattering is a very powerful technique for the observation of the spectrum in the low-frequency region.

C. Ferroelectric phase

In the FE phase, the Li and Ta ions are located at positions shifted along the Z axis from average positions in the PE phase that are shown by solid and dashed lines in Fig. 2(b), respectively.[9] Then, the point group symmetry of $LiTaO_3$ is C_{3v} in the FE phase and the irreducible representations of optical vibrational modes are

$$\Gamma_{\text{opt}}=4A_1(Z)+9E(X,Y)+5A_2,$$

where the A_1 and E modes are Raman, infrared and hyper-Raman active, whereas the silent A_2 modes are only hyper-Raman active. The soft mode has $A_1(Z)$ symmetry. The Raman tensors in the FE phase are given as follows:

$$A_1(Z)=\begin{bmatrix} a & \cdot & \cdot \\ \cdot & a & \cdot \\ \cdot & \cdot & b \end{bmatrix},$$

$$E(Y)=\begin{bmatrix} c & \cdot & \cdot \\ \cdot & -c & d \\ \cdot & d & \cdot \end{bmatrix},$$

$$E(X)=\begin{bmatrix} \cdot & c & d \\ c & \cdot & \cdot \\ d & \cdot & \cdot \end{bmatrix}.$$

On the other hand, the hyper-Raman tensors are given as follows:

$$A_1(Z)=\begin{bmatrix} a & -a/3 & \cdot & \cdot & b & \cdot \\ \cdot & \cdot & \cdot & b & \cdot & -a/3 \\ b & b & c & \cdot & \cdot & \cdot \end{bmatrix},$$

$$A_2=\begin{bmatrix} \cdot & \cdot & \cdot & \cdot & \cdot & -d/3 \\ -d/3 & d & \cdot & \cdot & \cdot & \cdot \\ \cdot & \cdot & \cdot & \cdot & \cdot & \cdot \end{bmatrix},$$

$$E(X)=\begin{bmatrix} e & e & g & \cdot & -f & \cdot \\ \cdot & \cdot & \cdot & f & \cdot & e \\ -f & f & \cdot & \cdot & g & \cdot \end{bmatrix},$$

$$E(Y)=\begin{bmatrix} \cdot & \cdot & \cdot & f & \cdot & e \\ e & e & g & \cdot & f & \cdot \\ \cdot & \cdot & \cdot & g & \cdot & f \end{bmatrix}.$$

Since the point group symmetry C_{3v} does not have centrosymmetry, SHG is allowed in the FE phase. The SHG tensor is given as follows:

$$\text{SHG}=\begin{bmatrix} \cdot & \cdot & \cdot & \cdot & m & -l \\ -l & l & \cdot & m & \cdot & \cdot \\ m & m & n & \cdot & \cdot & \cdot \end{bmatrix}.$$

Since the selection rule of SHG resembles that of the $A_1(Z)$ mode, the soft mode and hyper-Rayleigh scattering are often seen in the same spectra.

IV. RESULTS AND DISCUSSION

A. Central mode

1. Low-frequency spectra

Figures 3 and 4 show the central peak observed by hyper-Raman scattering at the $X(ZZZ)Y$ configuration in the high-temperature PE phase and the low-temperature FE phase, respectively. In the $X(ZZZ)Y$, the first two letters in the parenthesis indicate the polarization of the incident beams of light and the last letter indicates the polarization of the scattered light. The central peak could be observed up to about 1100 K in the 90° scattering configuration, but its detection becomes difficult above this temperature because of the strong thermal radiation. In the backscattering configuration, it could be done until about 1200 K because the slit height of the monochromator can be reduced. From the

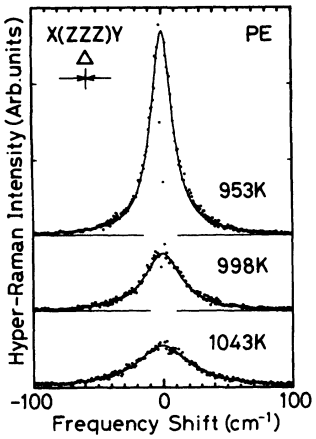

FIG. 3. Temperature dependence of the central mode by HRS measurement in the PE phase. The solid lines are Lorentzian line shapes.

configuration dependence of the central peak, the symmetry of this peak is $A_{2u}(Z)$ in the PE phase and $A_1(Z)$ in the FE phase. As shown later, the central peak has a Lorentzian-type line shape. The central-peak intensity grows up and the linewidth becomes narrower as the temperature approaches T_C in both phases. The intensity of the central peak in the PE phase is much stronger than that of the lattice modes, while in the FE phase is of the same order. A phonon band is observed around 60 cm^{-1} overlapping the central peak, in the FE phase, as shown in Fig. 5.

By means of Raman scattering, the central peak is observed only in the FE phase. Figure 5 shows a comparison between Raman and hyper-Raman spectrum at a temperature near T_C in the FE phase. The relative intensity of the central peak compared to the 200-cm^{-1} lattice mode is stronger in the hyper-Raman spectrum than in the Raman spectrum.

2. *Line-shape analysis*

The intensity $I(\omega)$ of the hyper-Raman scattering in the low-frequency region is given in the high-temperature

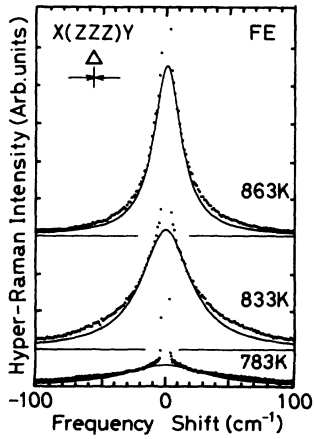

FIG. 4. Temperature dependence of the central mode by HRS measurement in the FE phase. The solid lines are Lorentzian line shapes. Additional multiphonon bands are observed at around 60 cm^{-1}.

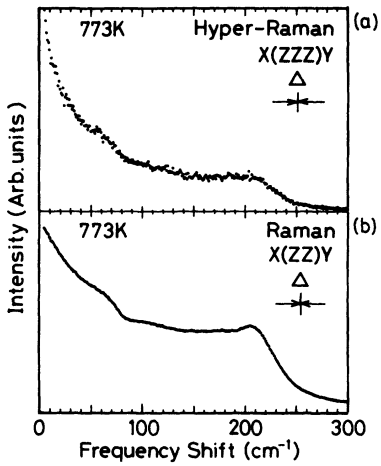

FIG. 5. Comparison between Raman (b) and hyper-Raman (a) spectra in the FE phase.

approximation as follows:

$$I(\omega)\sim\frac{kT}{\hbar\omega}\,\mathrm{Im}\chi(\omega)\ , \tag{1}$$

where $\mathrm{Im}\chi(\omega)$ is the imaginary part of the susceptibility.[13]

Assuming the order-disorder-type phase transition, the frequency dependence of $I(\omega)$ can be written as follows:

$$I(\omega)\sim\frac{kT}{\hbar}\chi(0)\frac{\tau}{1+(\omega\tau)^2}\ , \tag{2}$$

where τ is the relaxation time.[13] This equation shows that the line shape of $I(\omega)$ is a Lorentzian except for the temperature factor.

On the contrary, for the displacive-type phase transition with a damped harmonic oscillator, the line shape of $I(\omega)$ is given as follows:[13]

$$I(\omega)\sim\frac{kT}{\hbar}\chi(0)\frac{\omega_0^2\Gamma_0}{(\omega_0^2-\omega^2)^2+(\omega\Gamma_0)^2}\ , \tag{3}$$

where ω_0 and Γ_0 are the phonon frequency and the damping constant, respectively.

When the ratio $\Gamma^2/2\omega^2$ is larger than 1, the phonon mode becomes overdamped. Since the two line shapes of the Lorentzian and overdamped phonons are often very similar, it is very difficult to discriminate these. Thus, the frequency dependence of $I(\omega)\omega^2$ is useful to determine the spectral line shape of the observed $I(\omega)$.[13] If the spectral line shape is a Lorentzian, $I(\omega)\omega^2$ increases monotonously with increasing ω and reaches a constant value at the high-frequency region as shown by the inset (a) in Fig. 6. On the other hand, if the line shape is a damped harmonic oscillator, $I(\omega)\omega^2$ has a maximum at $\omega=\omega_0$, and then decreases with increasing ω, as shown by the inset (b) in Fig. 6.

Figure 6 shows the plot of $I(\omega)\omega^2$ in the PE phase at a temperature near T_C. The result clearly shows that this quantity reaches a constant value in the high-frequency region. Therefore, it is considered that the line shape of the central peak in $LiTaO_3$ is a Lorentzian line shape

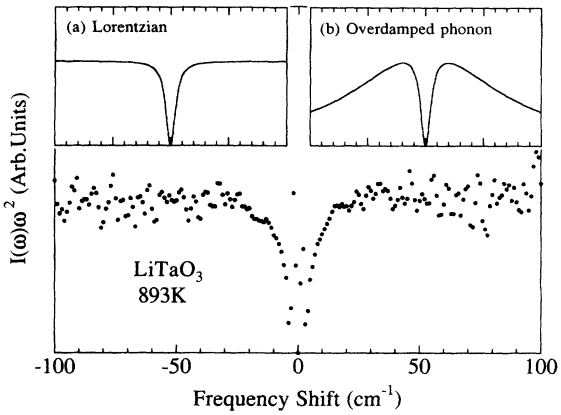

FIG. 6. Plot of $I(\omega)\omega^2$ where $I(\omega)$ is the intensity of the central mode observed at 893 K. (a) $I(\omega)\omega^2$ in the case of a Lorentzian spectrum. (b) $I(\omega)\omega^2$ in the case of an overdamped phonon spectrum.

within the experimental errors.

The log-log plot is also available to discriminate these two types of line shapes, since the spectrum becomes a straight line whose gradient is -2 for the Lorentzian and -4 for the overdamped phonon. Figure 7 shows the log-log plot of the central peak of $LiTaO_3$ in the PE phase. The spectrum shows a straight line with a gradient of -2. The spectrum clearly shows that this is a Lorentzian line shape given by Eq. (2).

3. Linewidth

Figure 8 shows the temperature dependence of the linewidth Γ of the central mode, which is equal to $1/\pi c\tau$, where c is the velocity of light. The linewidth in the PE phase is obtained by parameter fitting to Eq. (2) with the least-squares method. However, in the FE phase, the line shape of the observed central peak is not a simple Lorentzian because of the overlapping of the multiphonon band at about 60 cm^{-1}. Therefore, the line-shape fitting was carried out within the ± 30-cm^{-1} energy region.

As seen from Fig. 8, τ shows a linear temperature dependence on $(T-T_C)$ and is found to satisfy the Curie-Weiss law:

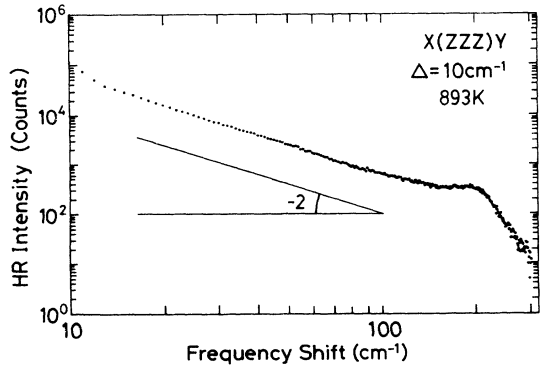

FIG. 7. log-log plot of hyper-Raman spectrum at 893 K in the PE phase. The gradient corresponds to the exponent of ω.

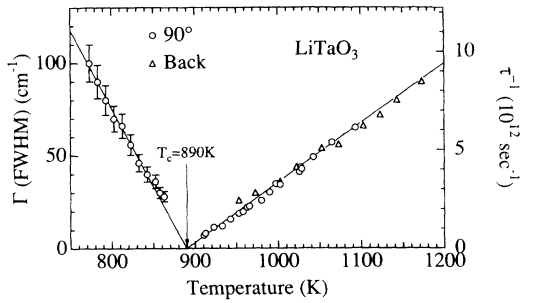

FIG. 8. Temperature dependence of Γ (FWHM) of the Lorentzian that corresponds to $1/\pi c\tau$. The solid lines are a guide to the eyes.

$$\tau = \frac{\tau_0 T_C}{|T-T_C|} , \tag{4}$$

with

$$\tau_0(\mathrm{PE}) = 3.7\times 10^{-14} \text{ sec}$$

and

$$\tau_0(\mathrm{FE}) = 1.2\pm 0.1\times 10^{-14} \text{ sec} .$$

That is, the phase transition of $LiTaO_3$ can be well described by the order-disorder-type transition.

4. Integrated intensity

Figure 9 shows the temperature dependence of the integrated intensity I_0 of hyper-Raman spectrum around 0 cm^{-1} that was measured by means of a spectral band pass of about 100 cm^{-1}. The intensity I_0 was observed in the $X(ZZZ)Y$ scattering configuration during a heating process for a poled single-domain sample.

It is clear as shown in Fig. 3 that the I_0 in the PE phase is almost due to the central mode. From the integration of Eq. (1), it is shown that the integrated intensity I_0 is proportional to $T\chi(0)$. Figure 10 shows the temperature dependence of the T/I_0 in the PE phase where I_0 is the integrated intensity at the (ZZZ) scattering configuration. Since the temperature dependence of

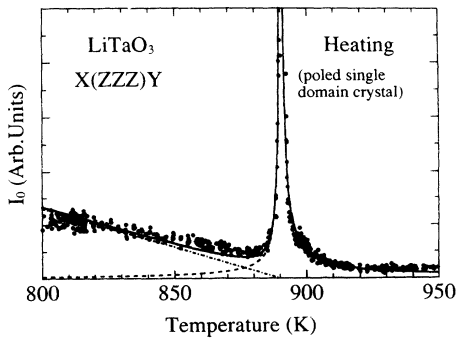

FIG. 9. Temperature dependence of integrated intensity I_0 of the central mode in a single-domain crystal of $LiTaO_3$ at the heating process. The dashed line shows the central mode component, the dash-dotted line shows the SHG component and the solid line shows the total intensity.

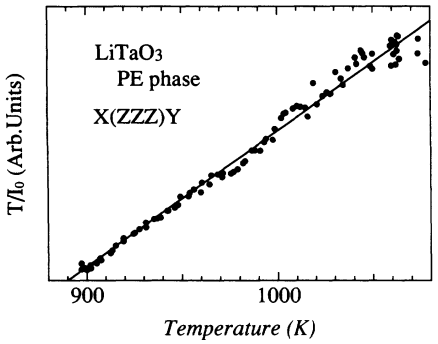

FIG. 10. Temperature dependence of T/I_0 that is proportional to the inverse susceptibility $1/\chi(0)$ in the PE phase. The solid line is a guide to the eyes.

T/I_0 is proportional to $(T-T_C)^{-1}$, the susceptibility $\chi(0)$ is found to obey the Curie-Weiss law.

In the case of the FE phase, I_0 decreases to zero monotonously as the temperature approaches T_C from lower temperature. Then, I_0 grows up rapidly in the vicinity of T_C in the FE phase. This divergence might be caused by the same reason in the PE phase. It is known that I_0 has two components;[14] central mode (I_c) and SHG ($I_{\rm SHG}$), i.e.,

$$I_0 = I_c + I_{\rm SHG} , \tag{5}$$

and I_c is expressed as follows.

$$I_c = \frac{CT}{|T-T_C|} , \tag{6}$$

where T is the temperature and C is a constant.

On the other hand, the intensity of SHG is known to be in proportion to the square of spontaneous polarization P_s.[15] According to Landau's phase-transition theory, the square of P_s is in proportion to $(T-T_C)$ near T_C, when the phase transition is of second order. Glass has found that the P_s of $LiTaO_3$ follows this theory.[16] Therefore, the intensity of SHG should decrease in proportion to $(T-T_C)$ in the FE phase, i.e.,

$$I_{\rm SHG} = D(T_C - T) , \tag{7}$$

where D is a constant. Then, I_0 is expressed as follows:

$$I_0 = \begin{cases} \dfrac{CT}{T_C - T} + \dfrac{D}{T_C - T} & (T < T_C) \\ \dfrac{C'T}{T - T_C} & (T > T_C). \end{cases} \tag{8}$$

In Fig. 9, the result of the fitting is shown as a solid curve. The calculated curve coincides well with the observed I_0 in the temperature region around T_C.

5. *The origin of the central mode*

Abrahams *et al.* found that the Li ion randomly distributes over either position of the equivalent sites that locate on both sides of the oxygen plane in the PE phase as shown in Fig. 2(d), while the Ta ion is located at an inversion center.[9] If the Li ion is flipping between these two equivalent positions, a central mode resulting from this motion will appear in the hyper-Raman spectra with a Lorentzian line shape. That is, the flipping motion of the Li ion is considered to dominate the phase transition.

B. A_1 lattice vibrational modes

1. *Ferroelectric phase*

Figure 11 shows the spectra observed by means of Raman and hyper-Raman scattering in (ZZ) and (ZZZ) scattering configurations, respectively. From the selection rules, these spectra should consist of four $A_1(Z)$ modes in the FE phase. However, more than four structures are seen in the spectra. For the Raman[2,4,17–19] and infrared[20] spectra, mode assignments were reported by many authors. Penna *et al.*[17] and Voron'ko *et al.*[18] assumed that the structure of $LiTaO_3$ is C_3 rather than C_{3v} symmetry in the FE phase, so that the $4A_1(Z)$ and silent $5A_2$ modes become Raman-active $9A(Z)$ modes. However, Yang *et al.* observed only four bands in Raman spectra at the backscattering configuration, and assigned these bands as $A_1(Z)$ phonon modes of the C_{3v} symmetry.[19] In this study, these four bands are observed at 203, 250, 355, and 596 cm^{-1}. Therefore, we believe that the symmetry of $LiTaO_3$ is C_{3v} rather than C_3, and that these four bands belong to A_1 phonons.

In the hyper-Raman spectrum at room-temperature (RT) [Fig. 11(c)], these four $A_1(Z)$ modes are clearly observed. The intensity of the 355-cm^{-1} structure is very weak, suggesting that this becomes the Raman-active and hyper-Raman-inactive modes in the PE phase.

2. *Paraelectric phase*

From group-theoretical analysis, it is shown that the four $A_1(Z)$ modes in the FE phase become one A_{1g} and

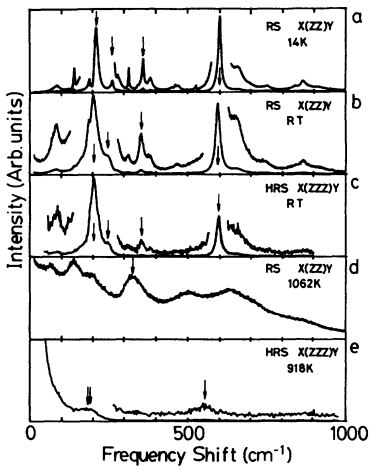

FIG. 11. Raman and hyper-Raman spectra of $LiTaO_3$. (a) RS at 14 K, (b) RS at RT, and (c) HRS at RT show the A_1 modes in the FE phase. (d) RS at 1062 K and (e) HRS at 918 K show the A_{1g} and A_{2u} modes in the PE phase, respectively. Arrows show the A_1 or A_{2u} mode.

three $A_{2u}(Z)$ modes in the PE phase. Figure 11(d) shows the Raman spectrum in the PE phase where one A_{1g} mode should exist. However, more structures are observed. Among these structures, the peak at 325 cm^{-1} has been assigned to A_{1g} mode by Raptis using several scattering configurations.[4] The other structures may be due to multiphonons.

Figure 11(e) shows the hyper-Raman spectrum in the PE phase with (ZZZ) scattering configuration. From factor group analysis, three $A_{2u}(Z)$ modes are expected to be observed at this configuration. However, in this hyper-Raman spectrum, only two phonon bands were observed at 190 and 555 cm^{-1} in addition to the very strong central mode. As discussed later, two bands are overlapping in the energy region of 190 cm^{-1}.

Prieto *et al.* reported that there is typically 0.6% oxygen vacancy in $LiTaO_3$.[21] The excess structures in Raman and hyper-Raman spectra may be explained in terms of the defect-induced spectra due to the oxygen vacancy.[22] Further, the weak SHG in the PE phase may be explained as the defect-induced SHG.[22]

C. Coupling between central mode and lattice mode

1. Coupling theory

Zhang *et al.* recently studied the low-frequency (ZZ) Raman spectra of $LiTaO_3$ in the FE phase at various temperatures and explained the spectral line shapes in terms of the coupling between a Debye-type relaxation mode and the lowest-frequency $A_1(Z)$ phonon.[23] They suggested that a Debye-type relaxation mode is caused by oxygen defects, which are not directly responsible for the phase transition. Tomeno *et al.* suggested from the study of dielectric properties of $LiTaO_3$ that the significant dispersions of susceptibility χ_{33} and conductivity σ_{33} are caused by the coupling between the soft phonon and either mobile defect or Li-ion motion.[11]

However, from this hyper-Raman measurement, it has been shown that the soft mode is the relaxational mode. Furthermore, the softening of the A_1 lattice mode could not be observed. However, anomalous line broadening of the A_1 lattice band at 203 cm^{-1} (RT) was observed. Thus, we assume the quantitative coupling system between the "pseudospin" and phonons, which has been proposed by Yamada *et al.*[24] In the theory, the "pseudospin" generally means the orientational ordering of the molecular groups. In the case of $LiTaO_3$, "pseudospin" may correspond to Li-ion flipping. The spectrum of the system is given as follows:

$$I(\omega)\sim A^2\Phi_{QQ}(\omega)+2AB\Phi_{Q\sigma}(\omega)+B^2\Phi_{\sigma\sigma}(\omega)\ , \qquad (9)$$

where Φ_{QQ}, $\Phi_{Q\sigma}$, and $\Phi_{\sigma\sigma}$ are correlation functions between phonon-phonon, phonon-spin, and spin-spin, respectively. Both "A" and "B" are constants including the Raman or hyper-Raman tensor. These correlation functions are[25]

$$\Phi_{QQ}(\Omega)\sim E(T)\frac{1-\bar{\tau}+\tilde{\omega}\tilde{\Gamma}\Omega^2+\tilde{\Gamma}(\tau^*+1-\bar{\tau})^2/\tilde{\omega}}{[\Omega^2-\tau^*/(\tau^*+1-\bar{\tau})]^2+\Omega^2[\tilde{\omega}(\Omega^2-1)/(\tau^*+1-\bar{\tau})-\tilde{\Gamma}]^2}\ ,$$

$$\Phi_{Q\sigma}(\Omega)\sim E'(T)\frac{(\Omega^2-1)-\tilde{\Gamma}(\tau^*+1-\bar{\tau})^2/\tilde{\omega}}{pp}\ ,$$

and

$$\Phi_{\sigma\sigma}(\Omega)\sim E''(T)\frac{(\Omega^2-1)^2-\tilde{\Gamma}(1-\bar{\tau})^2/\tilde{\omega}+\Omega^2\tilde{\Gamma}^2}{pp}\ ,$$

where

$$\bar{\tau}\equiv\frac{J(k)}{J(k)+g^2(k)},\quad \tilde{\omega}\equiv\omega_0\tau_0\ ,$$

$$\Omega\equiv\frac{\omega}{\omega_0},\quad \Gamma\equiv\frac{\Gamma_0}{\omega_0},\quad \tau^*\equiv\frac{|T-T_C|}{T_C}\ . \qquad (10)$$

The quantities ω_0 and Γ_0 are the characteristic frequency and damping of the phonon, respectively. The E, E', and E'' are the constants that are proportional to temperature T. The quantity τ_0 is the relaxation time of the flipping motion of individual spin when the coupling between spins and phonons is absent. The quantity T_C stands for the transition temperature, while $\bar{\tau}$ shows the ratio of the spin-phonon coupling $g^2(k)$ to the direct spin-spin coupling $J(k)$ as shown in Eq. (10). That is, $\bar{\tau}=0$ corresponds to the strong spin-phonon coupling limit, while $\bar{\tau}=1$ corresponds to the weak spin-phonon coupling limit. The parameter $\bar{\tau}$ mainly dominates the relative intensity of central mode and phonon in the spectra. The parameter $\tilde{\omega}$ shows the relative phonon frequency compared to the inverse of the spin relaxation time as shown in Eq. (10). That is, $\tilde{\omega}>1$ corresponds to the slow relaxation case (i.e., relaxation time of the pseudospin is slower than a period of the phonon vibration) while $\tilde{\omega}<1$ corresponds to the fast relaxation case (i.e., relaxation time of the pseudospin is faster than a period of the phonon vibration). The parameter $\tilde{\omega}$ mainly dominates the linewidth of the central mode.

2. Paraelectric phase

Figure 12 shows the fitting results of the hyper-Raman spectra by Eq. (9) in the PE phase. Since, in the PE phase, the hyper-Raman intensity of the $A_{2u}(Z)$ phonon band at about 190 cm^{-1} is very weak compared to that of the central mode, the parameter "A" is supposed to be zero, i.e.,

$$I(\omega)=B^2\Phi_{\sigma\sigma}(\omega)\ . \qquad (11)$$

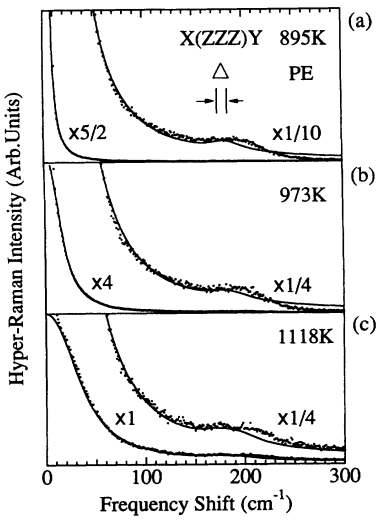

FIG. 12. Fitting result of Yamada's coupling system to the spectra of $LiTaO_3$ in the PE phase. The solid lines show coupling spectra by Yamada's system.

From the relative intensity between the central mode and the $A_{2u}(Z)$ phonon, $\bar{\tau}$ is obtained to be

$$\bar{\tau}\approx 0.7 .$$

Further, $\tilde{\omega}$ is obtained to be

$$\tilde{\omega}\approx 1.3 .$$

The temperature dependence of fitting constants in the PE phase is shown in Fig. 14.

The line-shape fittings are not very good in the higher-frequency side of the 190-cm^{-1} phonon band. As shown before, two phonon bands overlap at around 190 cm^{-1}. Since these two phonons have the same symmetry A_{2u}, they would couple with each other. Generally, the intensity decreases rapidly in the higher-frequency side of the bands, where the coupling takes place. Thus, the line-shape fitting will be better, if the coupling system includes all the relaxational modes and two phonon bands.

3. *Ferroelectric phase*

In the FE phase, both Raman and hyper-Raman spectra were fitted with the coupling system. Because two multiphonons are observed at 85 and 160 cm^{-1} (RT), we take these multiphonons into consideration. Figure 13 shows the fitting results of hyper-Raman spectra by Eq. (9) with two multiphonons in the FE phase. As shown by the dashed line, a central mode grows with increasing temperature, while the lowest-frequency $A_1(Z)$ phonon at 203 cm^{-1} does not become soft.

The multiphonon at 85 cm^{-1} varies in frequency gradually with increasing temperature and reaches 60 cm^{-1} at just below T_C. On the other hand, the damping of the multiphonon band increases with increasing temperature. Then the multiphonon becomes overdamped near T_C.

Another A_1 mode at 250 cm^{-1} decreases its frequency with increasing temperature and disappears around 200 cm^{-1} near T_C. From this fact, it is supposed that the

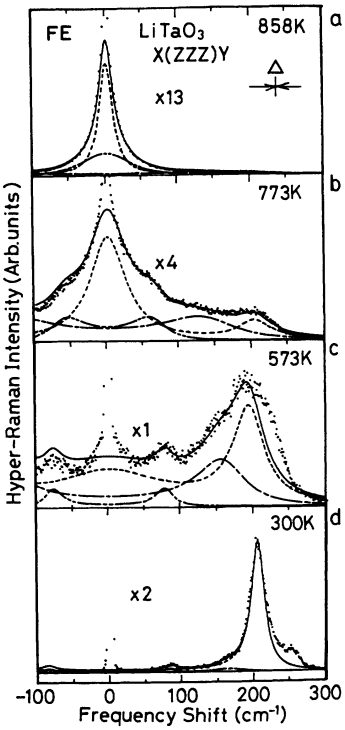

FIG. 13. Fitting result of Yamada's coupling system to the spectra of $LiTaO_3$ in the FE phase. The dashed broken lines show coupling spectra by Yamada's system, the two dash-dotted lines show the multiphonons, and the solid lines show the total line shapes.

broadband at about 190 cm^{-1} in the hyper-Raman spectrum in the PE phase [Fig. 11(e)] consists of two A_{2u} phonon bands.

The fitting parameters of Raman and hyper-Raman spectra are the same, except for the constant "A" and "B" in Eq. (9). The temperature dependence of the fitting constants in the FE phase is shown in Fig. 14. The parameters $\tilde{\omega}$ and $\bar{\tau}$ are almost constant at all temperatures. This result is different from the results obtained by Zhang *et al.*, where the coupling constant varies with temperature remarkably.[23] The parameter ω_0 of the optical $A_1(Z)$ phonon at 203 cm^{-1} (RT) varies slightly. The parameter Γ_0 increases linearly with increasing temperatures. This is consistent with the temperature dependence of the damping constant of other $A_1(Z)$ phonons.

In contrast to the hyper-Raman spectra in the PE phase that show strong central mode, the Raman spectra show rather strong $A_1(Z)$ phonon in the FE phase. Then, we supposed $B=0$, i.e.,

$$I(\omega)=A^2\Phi_{QQ}(\omega) . \tag{12}$$

From this result, it is considered that, in contrast to the hyper-Raman scattering in the PE phase, the Raman scattering in the FE phase is much more sensitive to Φ_{QQ} than $\Phi_{\sigma\sigma}$. From this fitting,

$$\tilde{\omega}\approx 0.7$$

and

$$\bar{\tau}\approx 0.8$$

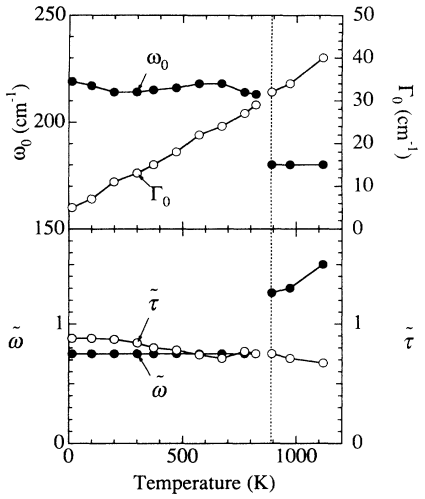

FIG. 14. Temperature dependence of fitting parameter $\tilde{\omega}$, $\tilde{\tau}$, ω_0, and Γ_0 in Yamada's system.

were obtained at all temperatures in the FE phase.

In the case of hyper-Raman scattering in the FE phase, the spectra show a more intensive central mode than the Raman spectra shown in Fig. 5. The spectra are thought to include Raman spectra, because strong SHG might induce a Raman scattering. As shown before, the hyper-Raman spectra in the PE phase could be explained by $\Phi_{\sigma\sigma}$ alone. Thus, the pure hyper-Raman spectra in the FE phase are supposed to be explained by $\Phi_{\sigma\sigma}$ alone. On the other hand, the SHG-induced Raman spectra are supposed to be explained by Φ_{QQ}. Then, the hyper-Raman spectra in the FE phase are explained by the linear combination of Φ_{QQ} and $\Phi_{\sigma\sigma}$ as Eq. (9). From this fitting, it is found that the ratio A/B decreases from about 2 (RT) to about 0.55 (near T_C). This result means the decreasing of Raman component with increasing temperature. As discussed before, the intensity of SHG decreases monotonously to zero as the temperature approaches T_C. Thus, the SHG-induced Raman spectra also decrease with increasing temperature. The variations of correlation function by experimental methods are summarized for both phases in Table I.

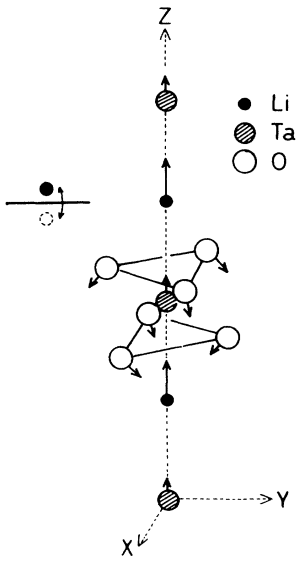

FIG. 15. Lattice vibrational mode of the lowest-frequency A_1 mode.

TABLE I. Correlation functions of $LiTaO_3$ in Yamada's system.

	FE	PE
Raman	Φ_{QQ}	
Hyper-Raman	$A^2\Phi_{QQ}+2AB\Phi_{Q\sigma}+B^2\Phi_{\sigma\sigma}$ ($B\rightarrow 0$ as $T\rightarrow T_C$)	$\Phi_{\sigma\sigma}$

4. *Meanings of the coupling parameters*

In this study, $\tilde{\omega}\approx 0.7$ and 1.3 were obtained in the FE and PE phases, respectively. These values are both classified into "intermediate" relaxation case in the coupling model of Yamada *et al.*, where the "intermediate" means that the phonon frequency and the damping constant of the central mode are comparable. Further, $\tilde{\tau}\approx 0.8$ and 0.7 were obtained in each phase. This value means a weak coupling between the phonon and central modes.

No drastic softening of the phonon was observed in this study. The A_1 phonon is thought to participate in the phase transition by the coupling with the central mode that dominates the dielectric anomaly. Figure 15 shows the vibrational displacements of the lowest $A_1(Z)$ phonon.[26] The displacements of the Li ions are along the Z axis. Thus, it is reasonable that the A_1 phonon couples with the flipping motion of the Li ion, if the Li ion flips between two equivalent positions on either side of oxygen plane.[9]

In the case of $BaTiO_3$, the soft phonon was observed by means of hyper-Raman scattering[25,27] in the PE phase. Vogt explained these spectra by the overdamped phonon alone.[27] On the other hand, Inoue and Akimoto analyzed these spectra using Yamada's formula [Eq. (9)], and got $\tilde{\omega}=2$ and $\tilde{\tau}=0.1$ that correspond to the rather slow relaxation and strong coupling case.[25] Because the soft phonon strongly couples with the relaxational mode, it becomes soft with a strong character of the overdamped phonon.

V. CONCLUSION

Raman and hyper-Raman scattering spectra of $LiTaO_3$ have been observed over the wide temperature range, including the phase transition temperature, from 14 to 1200 K. In the PE phase, a central mode is observed in the hyper-Raman spectra. It was found that the central mode has a Lorentzian-type line shape due to the Debye relaxation. The phase transition is well described by the order-disorder-type phase transition with the Debye relaxation mode. The relaxational mode might be caused by the Li-ion flipping motion as suggested by neutron-diffraction measurements.

In the FE phase, Raman scattering spectra show anomalous line shapes of the $A_1(Z)$ phonon mode, while

the spectra do not show any phonon softening. Then, the Raman spectra as well as the hyper-Raman spectra in both FE and PE phases are analyzed by the coupling theory between the central mode and phonon that is proposed by Yamada *et al.*[24] The Raman spectra are well described by Φ_{QQ} and the hyper-Raman spectra are well described by $\Phi_{\sigma\sigma}$. The coupling system can well elucidate the difference between the line shapes.

Then, the parameters $\bar{\omega}\approx 0.7$ and 1.3 were obtained in the FE and PE phases, respectively. These parameters mean that the relaxation time of the Li-ion flipping is comparable to a period of the phonon vibration. Further, the parameters $\bar{\tau}\approx 0.8$ and 0.7 show the weak coupling between phonon and central modes. Though the lowest $A_1(Z)$ phonon is recognized to be taking part in the phase transition through the coupling, the relaxational mode is dominant in the phase-transition mechanism of $LiTaO_3$.

[1]J. G. Bergman, A. Ashikin, A. A. Ballman, J. M. Levinstein, and R. G. Smith, Appl. Phys. Lett. **12**, 92 (1968).

[2]W. D. Johnston, Jr. and I. P. Kaminow, Phys. Rev. **168**, 1045 (1968).

[3]J. L. Servoin and F. Gervais, Solid State Commun. **31**, 387 (1979).

[4]C. Raptis, Phys. Rev. B **38**, 10 007 (1988).

[5]A. Jayaraman and A. A. Ballman, J. Appl. Phys. **60**, 1208 (1986).

[6]A. F. Penna, S. P. S. Porto, and A. S. Chaves, in *Light Scattering in Solids,* edited by M. Balkanski, R. C. C. Leite, and S. P. S. Porto (Flammarion, Paris, 1976), p. 890.

[7]A. F. Penna, S. P. S. Porto, and E. Wiener-Avnear, Solid State Commun. **23**, 377 (1977).

[8]E. J. Samuelsen and A. P. Grande, Z. Phys. B **24**, 207 (1976).

[9]S. C. Abrahams, E. Buehler, W. C. Hamilton, and S. J. Laplaca, J. Phys. Chem. Solids **34**, 521 (1973).

[10]M. R. Chowdhury, G. E. Peckham, and D. H. Saundersen, J. Phys. C **11**, 1671 (1978).

[11]I. Tomeno and S. Matsumura, Phys. Rev. B **38**, 606 (1988).

[12]Y. Tsuchiya, E. Inuzuka, T. Kurono, and M. Hosoda, Adv. Electron. Electron Phys. A **64**, 21 (1985).

[13]S. Shin, A. Ishida, T. Yamakami, T. Fujimura, and M. Ishigame, Phys. Rev. B **35**, 4455 (1987); S. Shin, Y. Tezuka, A. Sugawara, and M. Ishigame, Phys. Rev. B **44**, 11 724 (1991).

[14]S. Shin, Y. Tezuka, M. Ishigame, K. Deguchi, and E. Nakamura, Phys. Rev. B **41**, 10 155 (1990).

[15]R. C. Miller and A. Savage, Appl. Phys. Lett. **9**, 169 (1966).

[16]A. M. Glass, Phys. Rev. **172**, 564 (1968).

[17]A. F. Penna, A. Chaves, P. da R. Andrade, and S. P. S. Porto, Phys. Rev. B **13**, 4907 (1976).

[18]Yu. K. Voron'ko, A. B. Kudryavtesv, V. V. Osiko, A. A. Sobol', and E. V. Sorokin, Fiz. Tverd. Tela (Leningrad) **29**, 1348 (1987) [Sov. Phys. Solid State **29**, 771 (1987)].

[19]Xichen Yang, Guoxiang Lan, Bing Li, and Huafu Wang, Phys. Status Solidi B **141**, 287 (1987).

[20]A. S. Barker, Jr., A. A. Ballman, and J. A. Ditzenberger, Phys. Rev. B **2**, 4233 (1970).

[21]C. Prieto, L. Arizmendi, J. M. Cabrera, and J. A. Gonzalo, Ferroelectrics Lett. **3**, 81 (1985).

[22]S. Shin and M. Ishigame, Phys. Rev. B **34**, 8875 (1986).

[23]Ming-sheng Zhang and J. F. Scott, Phys. Rev. B **34**, 1880 (1986).

[24]Y. Yamada, H. Takatera, and D. L. Huber, J. Phys. Soc. Jpn. **36**, 641 (1974).

[25]K. Inoue and S. Akimoto, Solid State Commun. **46**, 441 (1983).

[26]A. S. Barker, Jr. and R. Louden, Phys. Rev. **158**, 433 (1967).

[27]H. Vogt, Proceedings of the Sixth International Meeting on Ferroelectricity, Kobe, 1985 [Jpn. J. Appl. Phys. Suppl. **24**, Suppl. 112 (1985)].

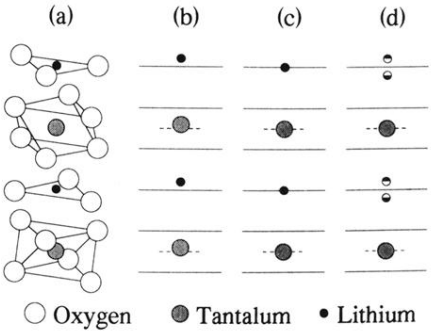

FIG. 2. (a) Structure of lithium tantalate. (b) Positions of Li and Ta ions in FE phase. (c) and (d) Positions of Li and Ta ions in the PE phase in the case of displacive-type phase transition (c) and order-disorder-type phase transition (d). Solid lines are the oxygen-ion plane. Dashed lines are the middle of the oxygen plane where the Ta ion is located.